



**Adaptive finite-element method for large-scale ab initio
molecular dynamics simulations**

Journal:	<i>Physical Chemistry Chemical Physics</i>
Manuscript ID:	CP-ART-01-2015-000320.R2
Article Type:	Paper
Date Submitted by the Author:	03-Apr-2015
Complete List of Authors:	Tsuchida, Eiji; National Institute of Advanced Industrial Science and Technology, Choe, Yoong-Kee; National Institute of Advanced Industrial Science and Technology, Ohkubo, Takahiro; Chiba University, Graduate School of Engineering

SCHOLARONE™
Manuscripts

Adaptive finite-element method for large-scale *ab initio* molecular dynamics simulations

Eiji Tsuchida and Yoong-Kee Choe

Nanomaterials Research Institute, National Institute
of Advanced Industrial Science and Technology (AIST),
Tsukuba Central 2, Umezono 1-1-1, Tsukuba 305-8568, Japan

Takahiro Ohkubo

Graduate School of Engineering, Chiba University,
1-33 Yayoi-cho, Inage-ku, Chiba 263-8522, Japan

Abstract

We present the current status of finite-element method for large-scale atomistic simulations based on the density-functional theory. After a brief overview of our formulation, we describe recent developments, including the optimal choice of adaptive coordinates, an efficient implementation of the ground-state calculations, and a remedy for the eggbox effect. As a **new** application of our formulation, we present *ab initio* molecular dynamics simulations on sulfonated poly(4-phenoxybenzoyl-1,4-phenylene) (SPPBP), which is a typical example of polymer electrolyte membranes for fuel cells.

I. INTRODUCTION

The finite-element method (FEM) has a long history in the field of engineering, and is often used to numerically solve partial differential equations such as the Navier-Stokes and Maxwell equations. This is mainly because FEM allows us to discretize these equations in a simple and flexible manner [1]. We can even go a step further and apply FEM to atomistic-to-continuum coupling [2–4]. In contrast, other basis sets, such as the plane waves [5] and atomic orbitals [6], have been traditionally preferred for the discretization of the Schrödinger equation (and its variants). However, real-space basis sets including FEM have recently attracted much attention [7], because these basis sets are optimal for electronic structure calculations on massively parallel computers.

The use of FEM for one- and two-dimensional Schrödinger equations dates back to the 1970s [8, 9]. Fully three-dimensional Hartree calculations on H, H₂⁺, He, and H₂ appeared in 1989 [10]. More recently, the adaptive grid was used for a single electron system [11], in which tetrahedral elements were used for discretization, and were divided recursively until sufficient accuracy was obtained.

FEM was also used for self-consistent calculations of many-electron systems within the density-functional theory by us [12]. We performed an all-electron calculation of H₂ and a pseudopotential calculation of bulk silicon. While our results were in good agreement with experiment and other calculations, the performance of our implementation was not competitive with that of plane-wave codes. Moreover, evaluation of the atomic forces was difficult. Therefore, we developed a more refined approach [13, 14] which is free from these drawbacks. An overview of this approach will be given in Sec.II, together with recent advances.

Soon after the publication of our works, extensions to general \mathbf{k} -point sampling [15] and time-dependent density-functional theory [16] were presented. Many research groups are now working on this topic, and significant progress has been made towards real-world applications in the last decade [17–30]. Several review articles are also available in the literature [7, 31].

The organization of the present paper is as follows. The building blocks of our approach are illustrated in Sec.II. The accuracy and performance of our implementation are evaluated in Sec.III. Our recent calculations on sulfonated poly(4-phenoxybenzoyl-1,4-phenylene) (SPPBP) at low hydration are introduced in Sec.IV. The conclusion is given in Sec.V.

II. THEORY

A. Overview

We first give a brief overview of our approach already described in detail in [previous publications](#) [13, 14]. Our code, FEMTECK (Finite-Element-Method-based Total Energy Calculation Kit), is based on the density-functional theory [32, 33] in the local density approximation or generalized gradient approximation [34]. Fully separable norm-conserving pseudopotentials are used to treat only the valence electrons explicitly [35, 36]. Periodic boundary conditions are applied in all directions, and only the Γ -point is used to sample the Brillouin zone, which allows us to consider only real-valued electron orbitals. The finite-element method is used to discretize the Kohn-Sham equations, and the orbitals are expanded by Hermite splines consisting of piecewise cubic polynomials. These basis functions are continuous up to first derivatives, complete to third order, and strictly localized in real space. These properties are crucial for rapid and systematic convergence with respect to the basis set size. The numerical integration involving these basis functions is performed using the Gauss-Legendre quadrature formula, which is considered the optimal choice for polynomial functions [37]. The Hartree potential is obtained by iterative solution of the Poisson equation for the charge density using the conjugate gradient method [37]. The multigrid method is used as a preconditioner for the conjugate gradient method to achieve rapid convergence as well as good parallel performance [38]. When we perform *ab initio* molecular dynamics (AIMD) simulations [39], the electron orbitals are quenched to the Born-Oppenheimer surface at each time step. In what follows, we describe other features of FEMTECK with emphasis on recent developments [40].

B. Adaptive curvilinear coordinates

The electron orbitals oscillate rapidly in the small regions near the nuclei, but vary much more slowly in other regions. Obviously, it is inefficient to use a uniform grid for the discretization of the Kohn-Sham equations, because the required spatial resolution is highly nonuniform. An attractive solution to this problem is to use the adaptive curvilinear coordinates first introduced by Gygi for electronic structure calculations [41]. In this approach, the grid changes continuously with atomic positions, which is crucial for molecular dynamics

and geometry optimization problems. We can also expect good parallel performance thanks to the perfect load balance.

Adaptation of the grid is given by a coordinate transformation of the form [42]:

$$\boldsymbol{\xi} = \mathbf{r} + \sum_i (\mathbf{r} - \mathbf{R}_i) g_i(|\mathbf{r} - \mathbf{R}_i|), \quad (1)$$

where the sum runs over all periodic images of the system, \mathbf{r} denotes the Euclidean coordinates, $\boldsymbol{\xi}$ the curvilinear coordinates, \mathbf{R}_i the atomic positions, and $g_i(r)$ is a scalar function to be discussed below. In FEMTECK, the electron orbitals are expanded by the finite-element basis functions on a uniform grid in $\boldsymbol{\xi}$ -space. We show the projection of a uniform grid in $\boldsymbol{\xi}$ -space onto \mathbf{r} -space for a diatomic molecule in Fig.1.

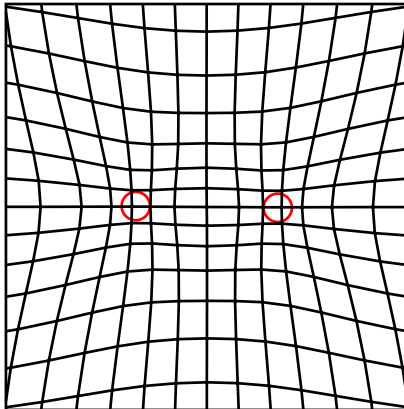


FIG. 1. Projection of a uniform grid in $\boldsymbol{\xi}$ -space onto \mathbf{r} -space for a N_2 molecule.

In the current implementation, we use the form

$$g_i(r) = A_i \left(1 + \left(\frac{r}{a_i} \right)^2 \right)^{-\frac{1}{2}} \exp \left[- \left(\frac{r}{b_i} \right)^2 - \left(\frac{r}{2b_i} \right)^4 \right], \quad (2)$$

where A_i and a_i are the strength and range of adaptation, respectively, and b_i determines the distance over which the influence of adaptation extends. The optimal parameters are mainly determined by the atomic density of the system, i.e., stronger adaptation is possible in the gas phase than in the condensed phase. However, the use of parameters optimized for the condensed phase gives acceptable results for the gas phase (but not vice versa). For simplicity, we assume that all atoms of the same element (e.g. hydrogen) have the same set of parameters, and the values of these parameters are kept fixed during the simulations.

Several authors have proposed elaborate strategies for finding the most efficient coordinate transformation in the past [41, 43, 44], but the optimal route is not yet established. Here we present an alternative method for determining the optimal parameters for adaptation. To this end, we first choose a typical atomic configuration, and define the objective function,

$$I(\Omega) = \sum_{i=1}^N |\mathbf{F}_i(\Omega) - \mathbf{F}_i^\infty|^2, \quad (3)$$

where N is the number of atoms in the system. Ω is a set of parameters to be optimized, where A_i and a_i are included in Ω , while b_i is determined manually for each element [45]. $\mathbf{F}_i(\Omega)$ is the force on the i -th atom for a given grid size, and \mathbf{F}_i^∞ is the force fully converged with respect to the grid size. In practice, we first calculate \mathbf{F}^∞ approximately using a very fine (non-optimized) adaptive grid (say, 10^4 or more basis functions per atom), followed by minimization of $I(\Omega)$ with respect to Ω in the spirit of the force matching method [46]. This approach aims at finding the optimal set of parameters which most faithfully reproduces \mathbf{F}^∞ for a given grid size. It is also possible to use two or more atomic configurations in the definition of $I(\Omega)$, which may be useful if the target system contains only a few atoms.

The minimization is performed by the downhill simplex method [37] which does not require the derivatives of $I(\Omega)$. The cost of parameter optimization is ~ 100 force evaluations. It is also worth noting that only a small subset of the target system is often sufficient to optimize the parameters. For instance, even if the target system consists of 1000 water molecules, it is justified to optimize the parameters (A_H, a_H, A_O , and a_O) for a system consisting of only 32 water molecules, assuming similar atomic densities. In our experience, the resolution near the nuclei can be enhanced by a factor of 2-2.5 in each direction without sacrificing the accuracy of other regions significantly. This level of enhancement is usually sufficient for pseudopotential calculations.

We note in passing that it is straightforward to calculate the atomic forces based on the Hellmann-Feynman theorem including the Pulay corrections arising from the adaptive coordinates [14, 42]. Although a significant programming effort is required, the computational cost is acceptable, because the influence of adaptation diminishes rapidly with distance from the nuclei.

C. Ground-state calculations

There are two common ways to obtain the ground-state energy and electron orbitals. The traditional approach is to solve the Kohn-Sham equation for a given potential, followed by repeatedly updating the potential until self-consistency is reached [5]. This approach is unfavorable for FEM, because nonorthogonality of the basis functions gives rise to a generalized eigenvalue problem, which is generally more expensive to solve. The second approach is the direct minimization of the total energy with respect to the coefficients of the basis functions [47]. We focus on the latter approach, which is particularly suited for a system with an energy gap.

In our earlier works, minimization of the total energy was performed iteratively using the nonlinear conjugate gradient method [37]. This method consumes only a small amount of memory, and requires, on average, two energy evaluations to find the optimal step size at each iteration. In contrast, the quasi-Newton method [48] requires only one energy evaluation per iteration, because the step size is automatically determined from the previous search directions. Moreover, the convergence rate of the quasi-Newton method is comparable to that of the conjugate gradient method. Therefore, the quasi-Newton method is widely used for geometry optimization problems [49]. However, the memory requirements are prohibitive for the ground-state calculations in a naive implementation of the quasi-Newton method.

Limited-memory BFGS (Broyden-Fletcher-Goldfarb-Shanno) method [50, 51] is a variant of the quasi-Newton method which requires much less memory than the original method, while retaining its convergence properties. In the current version of FEMTECK, the ground-state calculations are performed using the limited-memory BFGS method [52]. We also note that other low-memory variants of the quasi-Newton method have been applied to charge density mixing [5] and quantum chemical calculations [53].

The computational bottlenecks in each iteration of the total energy minimization are the orthonormalization and subspace rotation of the orbitals, which scale cubically with system size. If all orbitals are updated simultaneously, these operations can be performed as dense matrix computations using level-3 BLAS/LAPACK routines, which can achieve near-peak performance on almost any processor [54].

It is common practice to perform these operations in double precision (64-bit) arithmetic to obtain accurate results. On the other hand, single precision (32-bit) arithmetic is at least

twice faster on modern processors including the GPUs. Unfortunately, if the whole calculation is performed in single precision, the iteration fails in the early stages of minimization [55].

Recently, a novel method has been proposed to solve the linear systems accurately and efficiently in mixed precision arithmetic [56]. In this method, most of the operations are performed in single precision, while achieving double precision accuracy. In a similar spirit, the ground-state energy and electron orbitals can be obtained with double precision accuracy using mixed precision arithmetic [55]. For instance, the orthonormalization of the orbitals (Ψ) can be written as

$$\Psi_{\perp} = \Psi \cdot S^{-\frac{1}{2}} \quad (4)$$

in matrix form, where S is the overlap matrix of the orbitals and $S^{-\frac{1}{2}}$ is a triangular matrix obtained by Cholesky factorization of S . If this equation is rewritten as

$$\Psi_{\perp} = \Psi + \Psi \cdot \Delta \quad (5)$$

with $\Delta = S^{-\frac{1}{2}} - I$, and assuming that S and $S^{-\frac{1}{2}}$ are calculated in double precision, it is relatively safe to calculate the matrix product $\Psi \cdot \Delta$ in single precision. This is because the contribution from this term becomes progressively smaller as convergence is approached. Similarly, the subspace rotation as well as other operations can also be significantly accelerated by mixed precision arithmetic [55].

D. Eggbox effect

Ideally, the total energy of the system, E_{total} , should be invariant under any translation, denoted by \mathbf{T} :

$$E_{\text{total}}(\mathbf{R}_1 + \mathbf{T}, \mathbf{R}_2 + \mathbf{T}, \dots, \mathbf{R}_N + \mathbf{T}) = E_{\text{total}}(\mathbf{R}_1, \mathbf{R}_2, \dots, \mathbf{R}_N) \quad (6)$$

In most real space methods, however, E_{total} depends on \mathbf{T} because of the discretization errors. This *eggbox effect* [57, 58] is significantly suppressed by adaptation of the grid [13], but still persists, and can lead to erroneous results, e.g., in AIMD simulations. In particular, the dynamic properties often suffer from artifacts such as spurious peaks in the power spectra and overestimation of the self-diffusion coefficients.

A naive solution to this problem is the postprocessing method described below; we first perform an AIMD simulation to generate a trajectory, where the discontinuous changes in atomic positions caused by the periodic boundary conditions are appropriately corrected. The instantaneous position and velocity of the center of mass at each time step can be easily calculated as $\mathbf{R}_{\text{CM}} = \sum_i m_i \mathbf{R}_i / M$ and $\mathbf{V}_{\text{CM}} = \sum_i m_i \mathbf{V}_i / M$, where $M = \sum_i m_i$ and \mathbf{V}_i denotes the atomic velocities. Then, the whole trajectory is modified as follows:

$$\mathbf{R}_i \rightarrow \mathbf{R}_i - \mathbf{R}_{\text{CM}} \quad (7)$$

$$\mathbf{V}_i \rightarrow \mathbf{V}_i - \mathbf{V}_{\text{CM}} \quad (8)$$

If we use the modified trajectory for the analysis, most of the artifacts are removed. This procedure has been successfully applied in [previous studies by one of the authors](#) [59, 60]. This is mainly because the motion of the center of mass is usually in equilibrium with other degrees of freedom, and thus its kinetic energy is limited in size. However, when the accuracy of atomic forces is poor, the velocity of the center of mass can be very large, which leads to the violation of the equipartition theorem [61, 62].

Therefore, we have recently implemented an alternative method which applies the corrections on-the-fly. Although less pronounced than in AIMD, the eggbox effect also exists in classical simulations when the Poisson equation is solved numerically in real space. Skeel *et al.* proposed a simple yet effective method to overcome this problem [63]. In this method, the force on each atom is modified as follows:

$$\mathbf{F}_i^{\text{mod}} = \mathbf{F}_i - \frac{m_i}{M} \sum_j \mathbf{F}_j \quad (9)$$

If these modified forces are used to integrate the equations of motion, the total energy is conserved, while keeping the center of mass fixed. Definition of the temperature is also modified as

$$T^{\text{mod}} = \frac{2E_{\text{kin}}}{(3N - 3)k_{\text{B}}}, \quad (10)$$

where E_{kin} denotes the total atomic kinetic energy. This approach is working very well in preliminary simulations of several liquid systems.

III. BENCHMARKING

A. Accuracy

Here we evaluate the accuracy of our implementation for a small model system. To this end, we compare the Kohn-Sham total energies of a methane molecule obtained from FEMTECK with those from ABINIT, which is a widely used plane-wave code for electronic structure calculations [64]. The total energies were calculated with and without adaptation of the grid in FEMTECK. All calculations were performed within the local density approximation using the Pade approximation to the exchange-correlation functional [35], and the same norm-conserving pseudopotentials were employed in both codes [35]. We used a cubic supercell of length 10 Bohr, and only the Γ -point was used to sample the Brillouin zone. The carbon atom was placed at the center of the cell, (5,5,5), and the positions of the other hydrogen atoms (in Bohr units) were (5.0, 5.1, 7.1), (6.8, 5.0, 4.3), (4.0, 3.3, 4.3), and (4.0, 6.7, 4.3), representing a slightly distorted molecule.

The values of the total energy obtained from the two codes are compared in Fig.2. For all numbers of basis functions, the total energy from FEMTECK using a uniform grid is significantly higher than the other two. In contrast, FEMTECK using an adaptive grid gives the lowest values up to 50,000 basis functions, which corresponds to the typical accuracy required for AIMD. ABINIT gives the lowest values above this threshold, presumably because the plane waves are smoother than cubic polynomials used in FEMTECK. However, the total energy from ABINIT increases slightly with the number of plane waves beyond 300,000 basis functions. The origin of this violation of the variational principle is not clear at the moment. The most accurate results from the two codes agree to 9 significant digits (-16.0419904 Ryd), which demonstrates the reliability of our implementation.

B. Parallel performance

It is relatively straightforward to perform real-space electronic structure calculations on parallel computers [7]. Similarly to other real-space approaches, our implementation is based on a simple domain decomposition method, which results in almost perfect load balance among the processors [14]. The interprocessor communication required in this approach consists mainly of (i) global communication of a matrix of dimension equal to the number

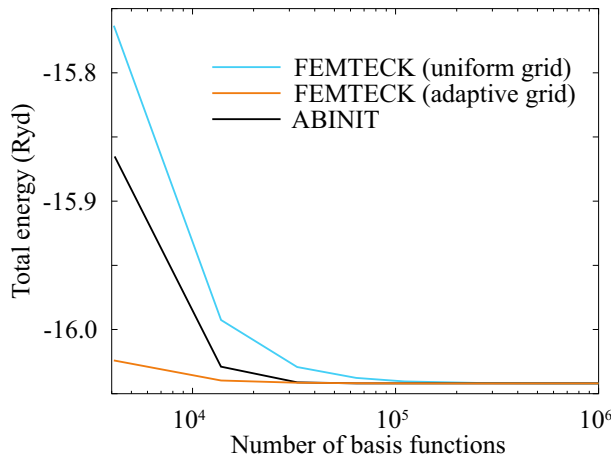


FIG. 2. Total energy of a methane molecule from FEMTECK and ABINIT.

of orbitals, and (ii) local communication of the boundary values of the orbitals between neighboring processors. The communication overhead can be minimized by overlapping communication and computation through the use of asynchronous communication.

The performance of FEMTECK on a parallel computer, Fujitsu FX10, which is based on the SPARC64 IXfx architecture, is discussed here. Each node of FX10 has 16 cores, 32 GB of memory, and a peak performance of 236.5 GFlops. We assigned one MPI (Message Passing Interface) process to each core of FX10, and measured the execution time for one AIMD step of the SPPBP system to be discussed in the next section on 16, 32, \dots , 512 cores. We used 32^3 elements to discretize the unit cell, and these elements were uniformly distributed over the cores. One AIMD step took 232 seconds on 16 cores, with a total memory requirement of 24.5 GB. Using this value as a reference, we show the parallel performance relative to the 16-core case in Fig.3. The speedup is found to be close to linear up to 512 processes.

IV. APPLICATIONS

Development toward commercialization of polymer electrolyte fuel cells (PEFCs) is ongoing nowadays because of their ability to convert chemical energy into electrical energy in a clean and sustainable manner [65]. A polymer electrolyte membrane (PEM) is an important component of PEFC whose role is to facilitate proton transport and maintain mechanical stability of membrane electrode assembly. As a proton conducting polymer electrolyte for PEFC applications, cheap hydrocarbon polymers have been developed and studied because

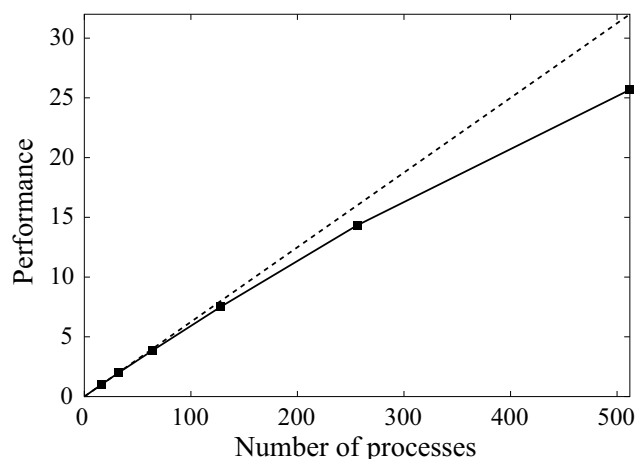


FIG. 3. Parallel performance of FEMTECK on Fujitsu FX10 for the SPPBP system discussed in Sec.IV. The dashed line shows the ideal speedup.

of their relatively low production cost and commercial availability compared with standard perfluoro type polymers such as Nafion [66]. A typical example of the polymers is sulfonated (poly ether ether ketone)s (SPEEK) [67–69]. Compared with Nafion, SPEEK tends to form much narrower water channels, which affects its performance for fuel cell applications [69]. SPPBP is another example of hydrocarbon membranes which is an isomer of SPEEK. SPPBP exhibits different water uptake and proton conductivity profiles in comparison with those of SPEEK [66]. One of the drawbacks of these hydrocarbon membranes is their poor proton conductivity under low hydration conditions [70]. Operation of PEFC under low or no water environment is highly desirable since, in such an environment, efforts for water management problem can be avoided. Thus, improvement of hydrocarbon PEM's performance under such a low hydration condition is of importance for the commercialization of PEFC.

In our previous paper, we have found that, in sulfonated poly ether sulfones (SPES), water molecules hydrate not only the sulfonate group ($-\text{SO}_3\text{H}$) but also the sulfone group ($-\text{SO}_2$) in the polymer [71, 72]. Moreover, in contrast to low-hydration Nafion, protons are not completely dissociated from the sulfonate groups in the case of SPES. These results indicate that the sulfone group has a negative effect that hinders the effective hydration around the sulfonate group, contributing to the poor proton transport of low hydration SPES. As shown in Fig.4, SPPBP has a carbonyl group which can make hydrogen bonds with water molecules or hydronium ions (H_3O^+). Thus, it is very likely that such a hydrophilic functional group

exerts a negative effect on the proton transport property of the PEM. In the present study, we have applied the AIMD simulation to SPPBP to investigate how molecular structure of SPPBP affects the proton transport at a low hydration condition.

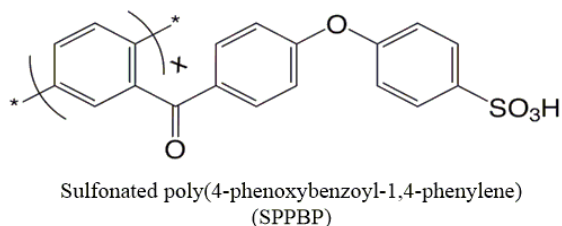


FIG. 4. Chemical Structure of SPPBP.

A snapshot from the AIMD simulation is presented in Fig.5 and details of simulation conditions are described in Table I. The degree of polymerization (x) for SPPBP is three, two of which are sulfonated. Thus, the total number of sulfonate groups in one SPPBP oligomer is two. We placed three SPPBP oligomers in a cubic unit cell of size 16.25 Å.

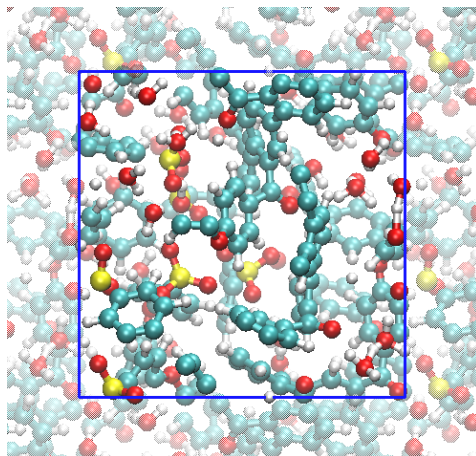


FIG. 5. Snapshot from AIMD simulation. Atom types are denoted by color as follows: red, oxygen; white, hydrogen; cyan, carbon; yellow, sulfur. Periodic images of atoms are also shown.

Since we are interested in proton transport under low hydration conditions, we considered the hydration level (λ) of 4, which corresponds to the minimum value required for proton transport in hydrated PEMs to occur [71, 73]. The density (1.32 g/cm³) of the hydrated SPPBP at $\lambda = 4$ was evaluated by the classical molecular dynamics simulation. The system was first equilibrated for 1 ns in the NVT ensemble, followed by a 5 ns NPT simulation. The final atomic configuration was used as the initial guess for the AIMD simulation. Fur-

ther details of the classical simulation are given in our previous paper [74]. In the AIMD simulation, the system was first equilibrated at high temperatures (above 1000 K), followed by annealing to the target temperature in 40 ps, during which period all intramolecular covalent bond lengths were kept fixed to avoid bond dissociation. Then, all constraints on the bond lengths were removed to allow the protons to dissociate from sulfonate groups. After a further equilibration of 10 ps, statistics were collected during the production run of 50 ps. The temperature was controlled by the Berendsen thermostat with a target temperature of 353 K. The hydrogen atoms were deuterated to use a time step of 1.21 fs in the production run. The atomic forces were evaluated using the Perdew-Burke-Ernzerhof functional [34] in conjunction with norm-conserving pseudopotentials and adaptive finite element basis sets.

TABLE I. Simulation conditions for hydrated SPPBP. Total number of atoms in a unit cell is 399.

Number of molecules in a unit cell	
SPPBP	3
H ₂ O	24
-SO ₃ H	6

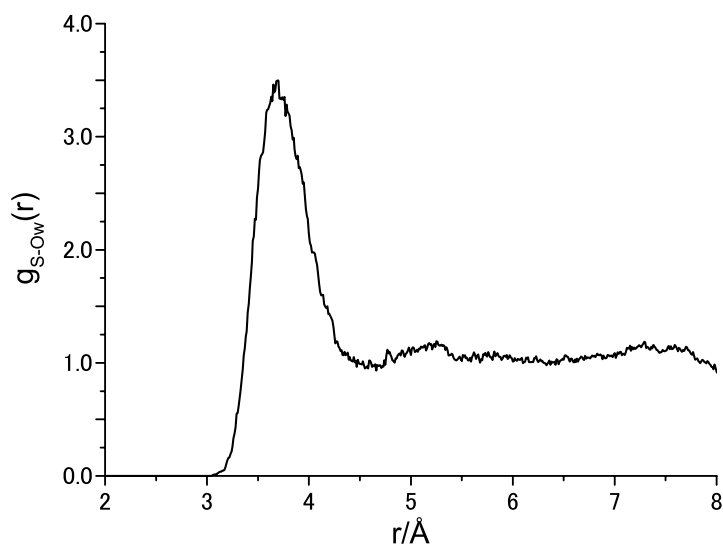


FIG. 6. RDF between the sulfur atom and O_w .

In Fig.6, we show the radial distribution function (RDF) between the sulfur atom and O_w , which denotes the oxygen atom of water molecules or hydronium ions. The first peak around 3.7 Å arises from hydrogen bonds between water molecules or hydronium ions and

the sulfonate group. Such a feature is very general for PEMs used in PEFCs, while the degree of hydration around the sulfonate group depends on the morphology and chemical structure of PEMs.

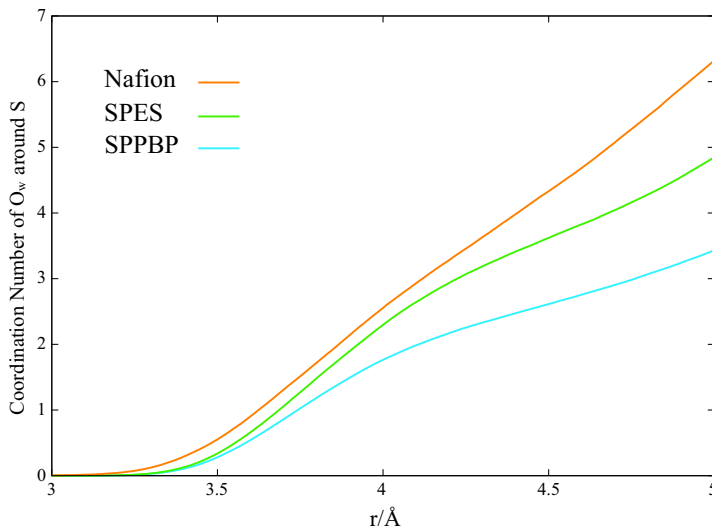


FIG. 7. Coordination numbers of O_w around the sulfur atom of the sulfonate group.

Fig.7 shows the dependence of coordination numbers on the distance between the sulfur atom of the sulfonate group and O_w . For comparison, we also plotted the coordination numbers of other PEMs with similar hydration levels ($\lambda = 4$ for SPES and $\lambda = 4.25$ for Nafion), taken from our previous studies [71, 75]. As shown in the figure, the coordination number of O_w is largest in the case of Nafion while that of SPPBP is smallest. This result indicates that water molecules or hydronium ions do not effectively hydrate the sulfonate group in SPPBP. As demonstrated in our previous study on SPES [71], such a poor hydration arises from a hydrophilic functional group which is able to make hydrogen bonds with water molecules or hydronium ions.

In Fig.8, RDF between the carbonyl oxygen atom and O_w is presented. The first peak in the RDF arises from the interaction between the carbonyl oxygen atom and O_w , indicating that some water molecules in the system participate in hydrating the carbonyl group. Since the solvation of the acidic group results in proton dissociation in PEMs, and thus facilitates proton transport, the carbonyl group hinders hydration around the sulfonate group by attracting water molecules to its vicinity. In other words, the above poor hydration of the sulfonate group in the case of SPPBP, to some extent, results from the fact that some water

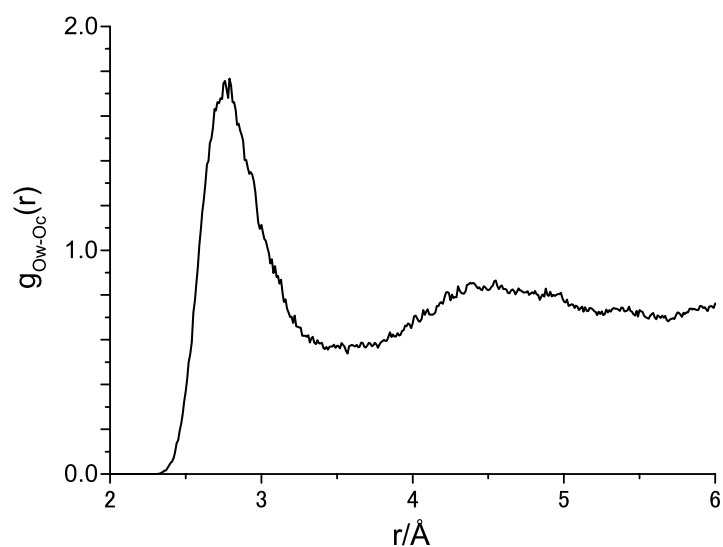


FIG. 8. RDF between the carbonyl oxygen atom and O_w .

molecules are trapped by the carbonyl group.

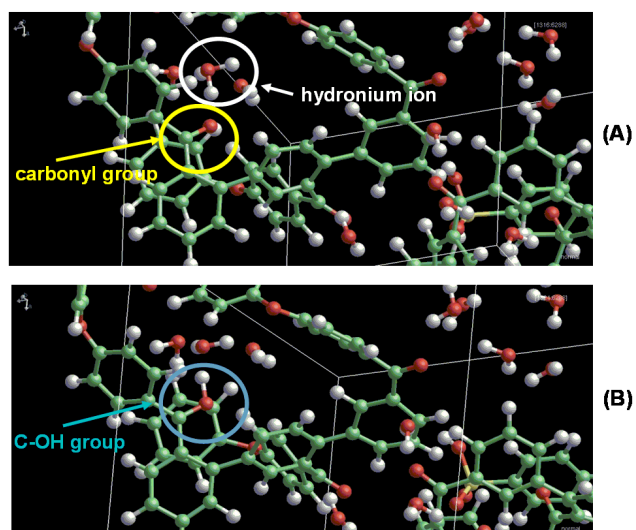


FIG. 9. (A) Snapshot from the AIMD simulation, where a hydronium ion is located next to the carbonyl group. (B) Another snapshot (about 50 fs after the configuration (A)) where the proton in the hydronium ion has been transferred to the carbonyl group.

Another interesting aspect of the carbonyl group's role in SPPBP can be found in Fig.9, where we present two snapshots of the trajectory obtained from the AIMD simulation. It is seen in Fig.9(A) that a hydronium ion is located next to the carbonyl group. One proton in the hydronium ion is then transferred to the neighboring carbonyl oxygen, as shown

in Fig.9(B). Thus, the carbonyl group is turned into -C-OH upon proton transfer from a hydronium ion. This result suggests that because of the carbonyl group, protons tend to be localized within the membrane, which eventually hinders the transport of protons.

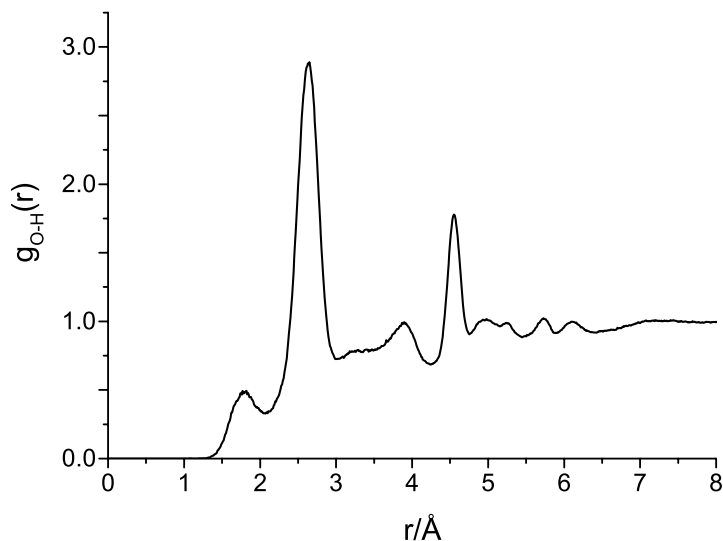


FIG. 10. RDF between the carbonyl oxygen atom and any hydrogen atom.

The above reaction is also confirmed by RDF between the carbonyl oxygen atom and any hydrogen atom, shown in Fig.10. The first peak around 1.7 Å arises, as described above, from the *intramolecular* atomic pair between the oxygen atom and the hydrogen atom in the CO-H moiety.

In summary, we have investigated properties of hydrated SPPBP at $\lambda = 4$ using the AIMD simulation. We found that the carbonyl group makes a negative influence on the proton transport in two ways: (i) The carbonyl group hinders the solvation around the sulfonate group by making hydrogen bonds with water molecules, and (ii) The carbonyl group is able to accept a proton, leading to the formation of -C-OH, which affects the transport of proton in a negative manner. We emphasize that such behavior is typically not captured by classical simulations.

V. CONCLUSIONS

We have presented the state-of-the-art of the finite-element method for electronic structure calculations within the density-functional theory. Following a brief historical survey, several new techniques were described in detail. **Results of our AIMD simulations** on SPPBP

at low hydration were also introduced. As we have shown in this article, FEM is sufficiently mature for real-world problems, and an AIMD simulation of 10^2 ps for a system containing up to 10^3 atoms is now a routine on a PC-cluster. Nevertheless, the time and length scales accessible to AIMD simulations are still far from satisfactory for industrial applications. In the last decade, we devoted considerable effort to this problem.

The length scale is limited by the computational bottlenecks which scale cubically with system size, and thus many algorithms have been developed for approximate solution of the Kohn-Sham equations with linear-scaling effort [76, 77]. We have recently proposed an efficient implementation of the linear-scaling method which is simple, efficient and robust [78]. The validity of this approach has been demonstrated in several applications, such as the static and dynamic properties of liquid ethanol at room temperature [60], and superionic conduction in the high-temperature phase of LiBH_4 [79]. This approach is particularly useful for systems containing more than 10^3 atoms. Multiscale modeling is another promising approach which has recently attracted much attention [2–4]. If we want to take into account the phase-separated morphology of the PEM in a fuel cell, for instance, multiscale modeling using the finite-element method would be a viable option.

The limited time scale is another serious problem which also arises in classical simulations [80]. This problem is difficult to overcome completely, but is significantly alleviated by efficient sampling of the phase space [81]. For instance, constrained molecular dynamics [82] and mass tensor molecular dynamics [83, 84] were found to accelerate AIMD simulations by up to a factor of three. We have also recently developed an effective method to stabilize the Verlet method at no extra cost [85]. Besides these methods, there are many other possibilities for accelerating AIMD simulations [86–88].

ACKNOWLEDGEMENTS

This work has been supported by the Strategic Programs for Innovative Research (SPIRE) and a KAKENHI grant (22104001) from the Ministry of Education, Culture, Sports, Science & Technology (MEXT), the Japan-US Cooperation Project for Research and Standardization of Clean Energy Technologies from the Ministry of Economy, Trade, and Industry (METI), and the Computational Materials Science Initiative (CMSI), Japan. Part of the calculations were carried out using the computer facilities at Research Institute for Infor-

mation Technology, Kyushu University.

- [1] C. Johnson, *Numerical Solution of Partial Differential Equations by the Finite Element Method*, Cambridge University Press, Cambridge, 1987.
- [2] R. Miller and E. Tadmor, *Model. Simul. Mater. Sci. Eng.*, 2009, **17**, 053001.
- [3] J. A. Templeton, R. E. Jones, J. W. Lee, J. A. Zimmerman, and B. M. Wong, *J. Chem. Theory Comput.*, 2011, **7**, 1736-1749.
- [4] M. Luskin and C. Ortner, *Acta Numerica*, 2013, **22**, 397-508.
- [5] W. E. Pickett, *Comp. Phys. Rep.*, 1989, **9**, 115-198.
- [6] A. Szabo and N. S. Ostlund, *Modern Quantum Chemistry*, McGraw-Hill, New York, 1989.
- [7] T. L. Beck, *Rev. Mod. Phys.*, 2000, **72**, 1041-1080.
- [8] M. Defranceschi and J. Delhalle, *Numerical Determination of the Electronic Structure of Atoms, Diatomic and Polyatomic Molecules*, NATO ASI Series C: Mathematical and Physical Sciences, Vol. 271, Kluwer, Dordrecht, 1989.
- [9] L. R. Ram-Mohan, *Finite Element and Boundary Element Applications to Quantum Mechanics*, Oxford University, Oxford, 2002.
- [10] S. R. White, J. W. Wilkins, and M. P. Teter, *Phys. Rev. B*, 1989, **39**, 5819-5833.
- [11] J. Ackermann, B. Erdmann, and R. Roitzsch, *J. Chem. Phys.*, 1994, **101**, 7643-7650.
- [12] E. Tsuchida and M. Tsukada, *Phys. Rev. B*, 1995, **52**, 5573-5578.
- [13] E. Tsuchida and M. Tsukada, *Phys. Rev. B*, 1996, **54**, 7602-7605.
- [14] E. Tsuchida and M. Tsukada, *J. Phys. Soc. Jpn.*, 1998, **67**, 3844-3858.
- [15] J. E. Pask, B. M. Klein, C. Y. Fong, and P. A. Sterne, *Phys. Rev. B*, 1999, **59**, 12352-12358.
- [16] N. Watanabe and M. Tsukada, *Phys. Rev. E*, 2002, **65**, 036705.
- [17] P. Motamarri, M. R. Nowak, K. Leiter, J. Knap, and V. Gavini, *J. Comput. Phys.*, 2013, **253**, 308-343.
- [18] V. Schauer and C. Linder, *J. Comput. Phys.*, 2013, **250**, 644-664.
- [19] G. Bao, G. Hu, and D. Liu, *J. Comput. Phys.*, 2015, **281**, 743-758.
- [20] P. Suryanarayana, K. Bhattacharya, and M. Ortiz, *J. Comput. Phys.*, 2011, **230**, 5226-5238.
- [21] J. Vackář, O. Čertík, R. Cimrman, M. Novák, O. Šipr, and J. Plešek, *Progress in Theoretical Chemistry and Physics*, 2012, **22**, 199-217.

- [22] T. D. Young, E. Romero, and J. E. Roman, *Comput. Phys. Commun.*, 2013, **184**, 66-72.
- [23] J. Fang, X. Gao, and A. Zhou, *J. Comput. Phys.*, 2012, **231**, 3166-3180.
- [24] A. Masud and R. Kannan, *Comput. Methods Appl. Mech. Engrg.*, 2012, **241**, 112-127.
- [25] L. Lin, J. Lu, L. Ying, W. E, *J. Comput. Phys.*, 2012, **231**, 2140-2154.
- [26] R. Alizadegan, K. J. Hsia, and T. J. Martinez, *J. Chem. Phys.*, 2010, **132**, 034101.
- [27] L. Lehtovaara, V. Havu, and M. Puska, *J. Chem. Phys.*, 2009, **131**, 054103.
- [28] E. J. Bylaska, M. Holst, and J. H. Weare, *J. Chem. Theory Comput.*, 2009, **5**, 937-948.
- [29] D. Zhang, L. Shen, A. Zhou, and X. Gong, *Phys. Lett. A*, 2008, **372**, 5071-5076.
- [30] J.-L. Fattebert, R. D. Hornung, and A. M. Wissink, *J. Comput. Phys.*, 2007, **223**, 759-773.
- [31] J. E. Pask and P. A. Sterne, *Model. Simul. Mater. Sci. Eng.*, 2005, **13**, R71-R96.
- [32] P. Hohenberg and W. Kohn, *Phys. Rev.*, 1964, **136**, B864-B871.
- [33] W. Kohn and L. J. Sham, *Phys. Rev.*, 1965, **140**, A1133-A1138.
- [34] J. P. Perdew, K. Burke, and M. Ernzerhof, *Phys. Rev. Lett.*, 1996, **77**, 3865-3868.
- [35] S. Goedecker, M. Teter, and J. Hutter, *Phys. Rev. B*, 1996, **54**, 1703-1710.
- [36] C. Hartwigsen, S. Goedecker, and J. Hutter, *Phys. Rev. B*, 1998, **58**, 3641-3662.
- [37] W. H. Press, S. A. Teukolsky, W. T. Vetterling, and B. P. Flannery, *Numerical Recipes in Fortran, 2nd Ed.*, Cambridge University Press, Cambridge, 1992.
- [38] O. Tatebe and Y. Oyanagi, in Proc. of Supercomputing '94, IEEE Computer Society, 1994, 194-203.
- [39] D. Marx and J. Hutter, *Ab Initio Molecular Dynamics: Basic Theory and Advanced Methods*, Cambridge University Press, Cambridge, 2009.
- [40] FEMTECK is currently used only by our close collaborators, but we plan to make it available to a broad range of users in the near future.
- [41] F. Gygi, *Phys. Rev. B*, 1993, **48**, 11692-11700.
- [42] F. Gygi, *Phys. Rev. B*, 1995, **51**, 11190-11193.
- [43] N. A. Modine, G. Zumbach, and E. Kaxiras, *Phys. Rev. B*, 1997, **55**, 10289-10301.
- [44] D. R. Hamann, *Phys. Rev. B*, 2001, **63**, 075107.
- [45] This is because the computational overhead associated with the adaptive grid grows cubically with b_i .
- [46] F. Ercolessi and J. B. Adams, *Europhys. Lett.*, 1994, **26**, 583-588.

- [47] R. M. Martin, *Electronic Structure: Basic Theory and Practical Methods*, Cambridge University Press, New York, 2004.
- [48] J. E. Dennis and R. B. Schnabel, *Numerical Methods for Unconstrained Optimization and Nonlinear Equations*, Englewood Cliffs, NJ, Prentice-Hall, 1983.
- [49] H. B. Schlegel, *WIREs Comput. Mol. Sci.*, 2011, **1**, 790-806.
- [50] D. C. Liu and J. Nocedal, *Math. Prog.*, 1989, **45**, 503-528.
- [51] P. E. Gill and M. W. Leonard, *SIAM J. Optim.*, 2003, **14** 380-401.
- [52] E. Tsuchida, *J. Phys. Soc. Jpn.*, 2002, **71**, 197-203.
- [53] M. Head-Gordon and J. A. Pople, *J. Phys. Chem.*, 1988, **92**, 3063-3069.
- [54] K. Goto and R. van de Geijn, *ACM Trans. Math. Softw.*, 2008, **35**, 1-14.
- [55] E. Tsuchida and Y-K. Choe, *Comput. Phys. Commun.*, 2012, **183**, 980-985.
- [56] M. Baboulin, A. Buttari, J. Dongarra, J. Kurzak, J. Langou, J. Langou, P. Luszczyk, and S. Tomov, *Comp. Phys. Commun.*, 2009, **180**, 2526-2533.
- [57] E. L. Briggs, D. J. Sullivan, and J. Bernholc, *Phys. Rev. B*, 1995, **52**, R5471-R5474.
- [58] E. Artacho, E. Anglada, O. Dieguez, J. D. Gale, A. Garcia, J. Junquera, R. M. Martin, P. Ordejon, J. M. Pruneda, D. Sanchez-Portal, and J. M. Soler, *J. Phys.: Condens. Matter*, 2008, **20**, 064208.
- [59] E. Tsuchida, *J. Chem. Phys.*, 2004, **121**, 4740-4746.
- [60] E. Tsuchida, *J. Phys.: Condens. Matter*, 2008, **20**, 294212.
- [61] S. C. Harvey, R. K.-Z. Tan, and T. E. Cheatham III, *J. Comput. Chem.*, 1998, **19**, 726-740.
- [62] S.-W. Chiu, M. Clark, S. Subramaniam, and E. Jakobsson, *J. Comput. Chem.*, 2000, **21**, 121-131.
- [63] R. D. Skeel, D. J. Hardy, and J. C. Phillips, *J. Comput. Phys.*, 2007, **225**, 1-5.
- [64] X. Gonze, B. Amadon, P.-M. Anglade, J.-M. Beuken, F. Bottin, P. Boulanger, F. Bruneval, D. Caliste, R. Caracas, M. Côté, T. Deutsch, L. Genovese, Ph. Ghosez, M. Giantomassi, S. Goedecker, D. R. Hamann, P. Hermet, F. Jollet, G. Jomard, S. Leroux, M. Mancini, S. Mazevet, M. J. T. Oliveira, G. Onida, Y. Pouillon, T. Rangel, G.-M. Rignanese, D. Sangalli, R. Shaltaf, M. Torrent, M. J. Verstraete, G. Zerah, J. W. Zwanziger, *Comput. Phys. Commun.*, 2009, **180**, 2582-2615.
- [65] F. Barbir, *PEM Fuel Cells: Theory and Practice*, Elsevier Academic Press, Burlington, 2005.
- [66] M. Rikukawa and M. Sanui, *Prog. Polym. Sci.*, 2000, **25**, 1463-1502.

- [67] Y.-Y. Zhao, E. Tsuchida, Y.-K. Choe, T. Ikeshoji, M. A. Barique, and A. Ohira, *Phys. Chem. Chem. Phys.*, 2014, **16**, 1041-1049.
- [68] G. Brunello, S. G. Lee, S. S. Jang, and Y. Qi, *J. Renewable Sustainable Energy*, 2009, **1**, 033101.
- [69] K. D. Kreuer, *J. Membr. Sci.*, 2001, **185**, 29-39.
- [70] K. D. Kreuer, *Solid State Ionics*, 1997, **97**, 1-15.
- [71] Y.-K. Choe, E. Tsuchida, T. Ikeshoji, A. Ohira, and K. Kidena, *J. Phys. Chem. B*, 2010, **114**, 2411-2421.
- [72] Y.-K. Choe, E. Tsuchida, T. Ikeshoji, A. Ohira, and K. Kidena, *ECS Trans.*, 2009, **25**, 1075-1083.
- [73] The hydration level is defined as the number of water molecules per sulfonate group.
- [74] T. Ohkubo, K. Kidena, N. Takimoto, and A. Ohira, *J. Mol. Model.*, 2011, **17**, 739-755.
- [75] Y.-K. Choe, E. Tsuchida, T. Ikeshoji, S. Yamakawa, and S. Hyodo, *Phys. Chem. Chem. Phys.*, 2009, **11**, 3892-3899.
- [76] D. R. Bowler and T. Miyazaki, *Rep. Prog. Phys.*, 2012, **75**, 036503.
- [77] T. Ozaki, *Phys. Rev. B*, 2006, **74**, 245101.
- [78] E. Tsuchida, *J. Phys. Soc. Jpn.*, 2007, **76**, 034708.
- [79] T. Ikeshoji, E. Tsuchida, T. Morishita, K. Ikeda, M. Matsuo, Y. Kawazoe, and S. Orimo, *Phys. Rev. B*, 2011, **83**, 144301.
- [80] D. E. Shaw, P. Maragakis, K. Lindorff-Larsen, S. Piana, R. O. Dror, M. P. Eastwood, J. A. Bank, J. M. Jumper, J. K. Salmon, Y. Shan, and W. Wriggers, *Science*, 2010, **330**, 341-346.
- [81] M. Christen and W. F. van Gunsteren, *J. Comput. Chem.*, 2008, **29**, 157-166.
- [82] E. Tsuchida and K. Terakura, *J. Phys. Soc. Jpn.*, 2001, **70**, 924-925.
- [83] C. H. Bennett, *J. Comput. Phys.*, 1975, **19**, 267-279.
- [84] E. Tsuchida, *J. Chem. Phys.*, 2011, **134**, 044112.
- [85] E. Tsuchida, *JPS Conf. Proc.*, 2015, **5**, 011019.
- [86] Y. Sugita and Y. Okamoto, *Chem. Phys. Lett.*, 1999, **314**, 141-151.
- [87] L. Baffico, S. Bernard, Y. Maday, G. Turinici, and G. Zérah, *Phys. Rev. E*, 2002, **66**, 057701.
- [88] D. Hamelberg, J. Mongan, and J. A. McCammon, *J. Chem. Phys.*, 2004, **120**, 11919-11929.